LRP 760/03 April 2003

Particle convection in TCV

- two papers -

I. Furno, H. Weisen, A. Zabolotsky
and TCV Team

ISSN 0458-5895

Table of contents

Observation of inward and outward particle convection in the core of ECH and ECCD plasmas in the TCV tokamak

I. Furno[1] and H. Weisen[2] and TCV team[2]
[1] *Los Alamos National Laboratory, M.S. E526, Los Alamos, NM 87545, USA*
[2] *Centre de Recherches en Physique des Plasmas, Association Euratom-Confédération Suisse, EPFL, Lausanne, Switzerland*
(Dated: February 4, 2003)

In TCV, inward or outward convection in the core of ECH and ECCD plasmas is observed, depending on discharge conditions. In sawtoothing discharges with central ECH, outward convection is observed when a quasi continuous $m = 1$ kink mode is present, resulting in inverted sawteeth on the central electron density, whilst in the absence thereof, inward convection between successive sawtooth crashes leads to 'normal' sawteeth. The occurrence of a kink mode depends sensitively on plasma triangularity. When sawteeth are stabilized with central Co- or Counter-ECCD, stationary hollow electron density profiles are observed in the presence of $m = 1$ modes, while peaked or flat profiles are observed in MHD quiescent discharges. The observation of peaked density profiles in fully EC driven plasmas demonstrates that pinch processes other than the Ware pinch must be responsible for these phenomena.

I. INTRODUCTION

In tokamak plasmas, particle transport is ordinarily characterized by an negative (inward-directed) convective velocity that results in moderately peaked density profiles. Electron cyclotron heating (ECH) and current drive (ECCD) appear to be at the origin of unexpected transport phenomena which are potentially important in the confinement of fusion plasmas. On TCV, in the presence of sufficiently high central ECH or ECCD power and a kink distortion of the plasma core, the direction of the convective component of particle flux can reverse (outward-directed). In sawtoothing discharges, the outward convection results in inverted sawteeth on the central electron density whereas, when sawteeth are stabilized with central Co- or Counter-ECCD, stationary hollow electron density profiles are observed. This can be, at least qualitatively, explained by neoclassical thermodiffusion arising from the presence of locally trapped particles due to magnetic field modulation in the central plasma region. The field modulation may result from the helical displacement of the plasma core, resulting from MHD instabilities affecting the plasma core, especially $m/n = 1/1$ kink modes or magnetic islands developing on the $q = 1$ surface.

In this article, we report on observation of inward and outward particle convection from the core of TCV plasmas and correlated mode activity during central ECH and ECCD. The remainder of the article is organized as follows. In Sec. II, the TCV tokamak, the relevant diagnostics and data analysis methods are briefly reviewed. Experimental observations are presented in Sec. III and an interpretation based on neoclassical thermodiffusion is discussed in Sec. IV. Finally, conclusions are summarized in Sec. V.

II. EXPERIMENTAL SETUP AND DIAGNOSTICS

TCV is a tokamak with major radius $R = 0.88$ m, minor radius $a = 0.25$ m, vacuum vessel elongation $\kappa = 3$ and vacuum central magnetic field $B \leq 1.54$ T[1]. TCV is equipped with 16 independently controlled poloidal field coils which allow for a large variety of plasma shapes. The TCV electron cyclotron (EC) system provides 3 MW of EC power for heating and current drive at the second cyclotron harmonic resonance (82.7 GHz) using the extraordinary mode[2]. The launching mirrors are separately orientable in the poloidal (during a discharge) and toroidal (between discharges) direction. The position of the wave absorption region and the total absorbed power are determined by the ray-tracing code TORAY[3].

Mode activity in the central region of the plasma is particularly visible on soft x-ray measurements. The TCV soft x-ray tomographic system consists of ten cameras at the same toroidal location, each equipped with a 47 μm beryllium filter and a linear array of 20 silicon photodiodes[4]. The system allows high time resolution (13 μs sampling rate) measurements of the electromagnetic radiation emitted from the plasma in the range $1 - 10$ keV. The local soft x-ray emissivity distribution is reconstructed from the line integrated measurements by means of the Minimum Fisher Information regularization method on a grid of 3 cm wide square pixels[5]. The time sequences of the reconstructed emissivities, $S_X(r,t)$, are analysed using the Singular Value Decomposition (SVD) method[6] to obtain the spatial structures u_k (topos) and their corresponding temporal evolution v_k (chronos) such that $S_X(r,t) = \sum u_k(r)v_k(t)s_k$, where s_k are the singular values. Structures with poloidal mode numbers up to $m = 3$ are resolved by the SVD and coherent rotating structures such as MHD modes can be identified. The SVD method also provides a reliable tool in the determination of the sawtooth inversion surface of the local soft x-ray emissivity, as well as the displacement of the plasma

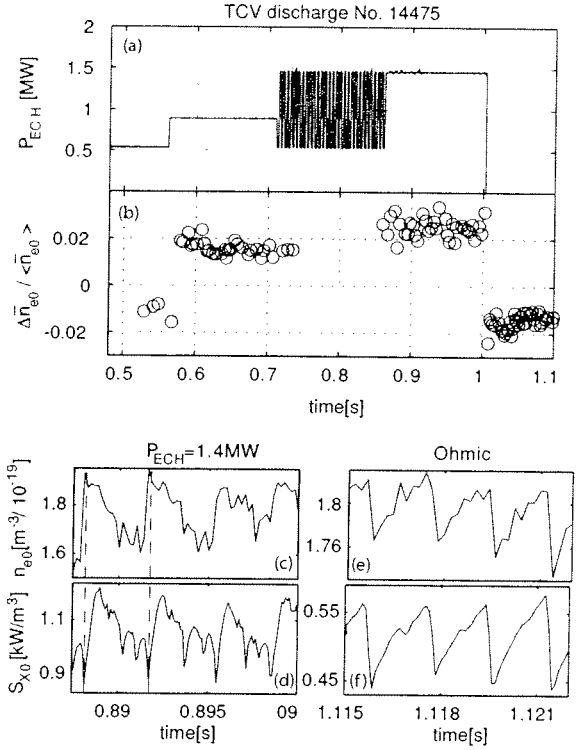

FIG. 1: Plasma response during sawtooth activity to different levels of injected ECH power and Ohmic heating only. The ECH resonance position is located inside the sawtooth inversion radius. Top traces show the stepping up of the ECH power (a) and the relative variation of $\overline{n}_{e0}$ at the sawtooth crash (b). Bottom traces show the temporal evolution of the central electron density and soft x-ray emissivity with 1.4 MW of ECH power (c,d) and Ohmic heating only (e,f). Dashed lines (c,d) indicate the time interval in which the SVD analysis is applied to inverted soft x-ray emissivities which is shown in Fig. 3

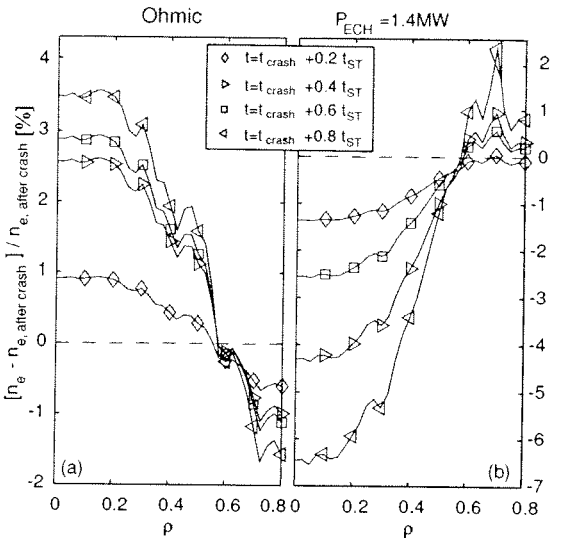

FIG. 2: Temporal evolution of the electron density profile during a sawtooth period for P_{ECH} = 1.4 MW and Ohmic heating only. A background subtraction of the profile just after the sawtooth crash, $n_{e,aftercrash}$, is applied to improve the visibility of the temporal evolution.

core in the presence of MHD perturbations[7]. The soft x-ray emission is also monitored by four toroidally equispaced silicon photodiodes (50 μm beryllium filter, 250 kHz acquisition frequency) placed at the top of the vessel and viewing the plasma along chords intersecting the poloidal midplane at a distance about 7 cm from the center of the vessel. These are used to determine toroidal mode numbers $n = 1, 2$ assuming there is no aliasing from toroidal mode numbers $n \geq 3$.

A 14-chord far infrared interferometer (FIR) provides measurements of the line integrated electron density with a sufficiently high temporal resolution (150 μs sampling rate) to resolve the particle transport. Local electron density profiles are reconstructed from line integrated measurements by means of a modified Abel inversion method taking into account the non-circular shape of TCV plasmas[8]. The line integrated central electron density is also monitored by a microwave interferometer (50 μs sampling rate) operating at 140 GHz. A 25-point, triple laser, multipulse Thomson scattering system provides profiles of the electron temperature and density with a spatial resolution of 40 mm in vertical direction and 3 mm in radial and toroidal directions. Typical sampling rates are in the range 20 – 60 Hz depending on the laser synchronization[9].

III. EXPERIMENTAL OBSERVATIONS

In Fig. 1, the plasma response to a stepping up of the injected ECH power is presented during sawtooth activity. Plasma parameters are $\delta_a = 0.23$, $\kappa_a = 1.54$, $I_P = 393$ kA, $q_a = 2.9$. The ECH resonance position is located inside the sawtooth inversion radius and P_{ECH} is increased in three steps from 0.5 MW to 1.4 MW, Fig. 1(a). In Fig. 1(b), the relative variation of the central line integrated density at the sawtooth crash is defined as $\Delta\overline{n}_{e0}/\langle\overline{n}_{e0}\rangle$, where the brackets $\langle\rangle$ indicate the average of a quantity evaluated before and after the sawtooth crash and is determined from an interferometric chord looking through the plasma center. Negative values of $\Delta\overline{n}_{e0}/\langle\overline{n}_{e0}\rangle$ are associated with the collapse of a peaked density profile and are observed during 'normal' sawteeth (see below). Positive values of $\Delta\overline{n}_{e0}/\langle\overline{n}_{e0}\rangle$ are observed in the ECH case for $P_{ECH} \geq 0.8$ MW and are suggestive of a sudden flattening of hollow density profiles at the sawtooth crash. The creation of a hollow density profile just before the crash, instead of the usual peaked profile, implies the reversal of the direction of particle

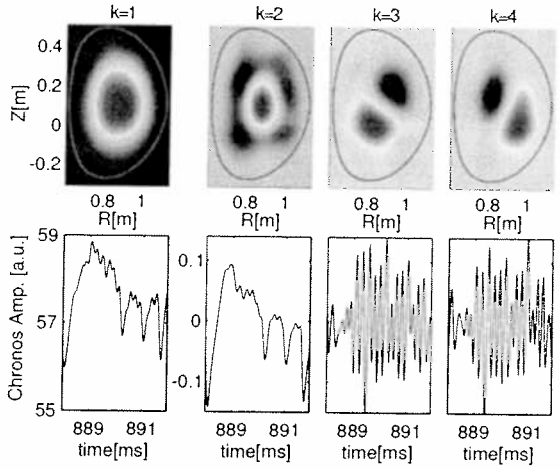

FIG. 3: SVD analysis of the reconstructed soft x-ray emissivities during the phase shown in Fig. 1(c) by dashed lines. Shown are the topo/chrono pairs corresponding to four largest eigenvalues. The top row shows the spatial eigenmodes (topos) with the last close flux surface. The corresponding temporal eigenvectors (chronos) are shown in the bottom row.

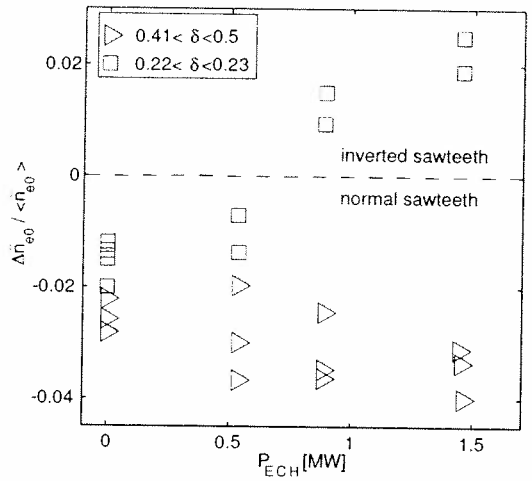

FIG. 4: Relative variation of $\overline{n}_{e0}$ at the sawtooth crash for different plasma triangularity and injected ECH power. Positive and negative values indicate respectively inverted and normal sawteeth.

convection from inward to outward during the sawtooth ramp phase. In the same figure, bottom rows give an expanded view of sawtooth oscillations for $P_{ECH} = 1.4$ MW and Ohmic heating only. The temporal evolution of the Abel-inverted central electron density n_{e0}, Fig. 1(c, e), is shown together with the tomographically inverted central soft x-ray emissivity S_{X0}, Fig. 1(d,f). For the same discharge, the temporal evolution of the electron density profile during a sawtooth period is shown for $P_{ECH} = 1.4$ MW, Fig. 2(b), and Ohmic heating only, Fig. 2(a).

In the Ohmic case, 'normal' sawteeth, i.e. triangular shaped sawteeth, are observed, Fig. 1(e,f). Both n_{e0} and S_{X0} increase during the sawtooth ramp and then drop at the sawtooth crash on a fast time scale (typically $\tau_{crash} \leq 100$ μs) resulting in a normalized crash amplitude $\Delta\overline{n}_{e0}/\langle\overline{n}_{e0}\rangle \approx -1.5\%$. After the sawtooth crash, the increase of n_{e0} results from a particle flux in the direction of the density gradient and hence from an inward particle convection, as shown by the temporal evolution of the electron density profile in Fig. 2(a). During this phase, the soft x-ray emissivity profile (not shown here) is poloidally symmetric with no detectable MHD mode activity.

For this plasma shape, the central ECH deposition strongly perturbs the triangular ohmic sawteeth. With $P_{ECH} \geq 0.8$ MW, a negative sawtooth ramp (inverted sawtooth) of both n_{e0} and S_{X0} is observed. The case $P_{ECH} = 1.4$ MW is shown in Fig. 1(c,d). During the inverted sawtooth ramp, the decrease in n_{e0} results from an outward flux, which, in the region of the hollow profile, is in the same direction as the density gradient, and hence corresponds to net outward convection, as shown in Fig. 2(b). This results in a slight hollowing of the electron density profile, with $n_{e,max}/n_{e0} \approx 1.04$ at the end of the sawtooth ramp, followed by a fast recovery at the sawtooth crash. The relative amplitude of the recovery of the line integrated density $\Delta\overline{n}_{e0}/\langle\overline{n}_{e0}\rangle$ increases from 1.6% at $P_{ECH} = 0.8$ MW to 2.3% at $P_{ECH} = 1.4$ MW, Fig. 1(b). The presence of normal sawteeth for $P_{ECH} = 0.5$ MW suggests the existence of a power threshold for reversing the sign of the particle convection. During the inverted sawtooth ramp phase, quasi-continuous $m/n = 1/1$ mode activity is observed, as shown in Fig. 3. In this figure, the mode structure of the soft x-ray emissivity, from Singular Value Decomposition (SVD), is shown in the time interval indicated in Fig. 1(c) by dashed lines. Inspection of Fig. 3 reveals the presence of a rotating $m = 1$ mode at a frequency of ≈ 5 kHz (topos/chronos pairs $k = 3, 4$). The toroidal mode number, as obtained from toroidally spaced soft x-ray photodiodes, is $n = 1$. Partial collapses of the soft x-ray emissivity are observed during the negative sawtooth ramp, which result in a flattening of the soft x-ray profile (topos/chronos pair $k = 2$). The overall decrease of the soft x-ray emission, visible on the $k = 1$ component during the ramp phase, is due to its strong dependence on the electron density[8].

Figure 4 shows the crash amplitude from an ECH power scan for low and high triangularity obtained from a line integrated central electron density signal. At high triangularity, inward particle convection is observed. It is a generally observed feature in TCV, both in Ohmic [10] and ECH plasmas [11], that pre-and post-cursor mode activity is absent at high triangularity and increases in amplitude and duration as triangularity is reduced, sug-

gesting a link between mode activity and the observed particle transport.

The presence of an outward particle convection does not depend on the parallel velocity of the electrons interacting with the microwave beams and is observed on TCV with central Co- and Counter-ECCD as shown by the electron density profiles in Fig. 5(a,b). In Fig. 5(a,c) electron density and temperature profiles are shown in a case of full current replacement with Co-ECCD [12] at an injected power $P_{EC} = 2.7$ MW and plasma parameters: $\delta_a = 0.42$, $\kappa = 1.62$, $q_a = 7.8$, $I_P = 200$ kA. For the same discharge, the temporal evolution of the line integrated central soft x-ray emissivity $\overline{S}_{X0}$, Fig. 6(a), together with the line integrated central electron density $\overline{n}_{e0}$, Fig. 6(b), from a microwave interferometer operating at 140 GHz are shown during four sawtooth cycles. The outward particle transport is suggested by the inverted sawtooth ramp of $\overline{n}_{e0}$, Fig. 6(b), and results in density profiles which, unlike the ECH cases discussed above, are hollow enough ($n_{e.max}/n_{e0} \approx 1.4$) to be measured by the Thomson scattering system, Fig. 5(a), during most of the sawtooth cycle. A reliable tomographic inversion of the line integrated soft x-ray signals was hampered by x-ray emission from carbon tiles of the TCV vessel probably due to impacts of suprathermal electrons. Thus, no satisfactory tomographic inversion was obtained.

Nevertheless, the presence of a kink distortion of the plasma core is revealed during the inverted sawtooth ramp by slightly off-axis oscillations (not shown here) in the soft x-ray emissivity at a frequency of ≈ 3 kHz. The oscillations on line integrated soft x-ray signals along lines of sight viewing the plasma on different sides of the magnetic axis have opposite phase. This indicates a $m = 1$ poloidal mode number. The presence of a $m = 1$ mode during the inverted sawtooth ramp is also suggested by the displacement of the electron temperature profile, as shown in Fig. 5(c) by two profiles measured at different times during this phase, and by strong oscillations of the line integrated central $\overline{n}_{e0}$ electron density. The frequency of these oscillations is ≈ 3 kHz and the relative amplitude $\Delta\overline{n}_{e0}/\overline{n}_{e0} \approx 4\%$. In Fig. 5(b), the relative amplitude of the n_{e0} oscillations is artificially reduced by a factor of 8 by digitally filtering to improve the visibility of the inverted sawtooth ramp.

Figure 5(b) shows a hollow density profile ($n_{e.max}/n_{e0} \approx 1.3$) from an experiment with central Counter-ECCD with plasma parameters: $\delta = 0.25$, $\kappa = 1.71$, $q_a = 7.6$, $I_P = 220$ kA. In this discharge, which has no sawteeth, a continuous saturated $m/n = 1/1$ mode is present as shown in Fig. 7 by the SVD analysis of the inverted soft x-ray emissivities. This mode rotates at a frequency of ≈ 3 kHz and results in a helical displacement of the plasma core of ≈ 1 cm as determined from the reconstructed soft x-ray emissivities. The mode activity results also in oscillations of the line integrated central electron density (not shown here) at the frequency of ≈ 3 kHz and relative amplitude $\Delta\overline{n}_{e0}/\overline{n}_{e0} \approx 1\%$.

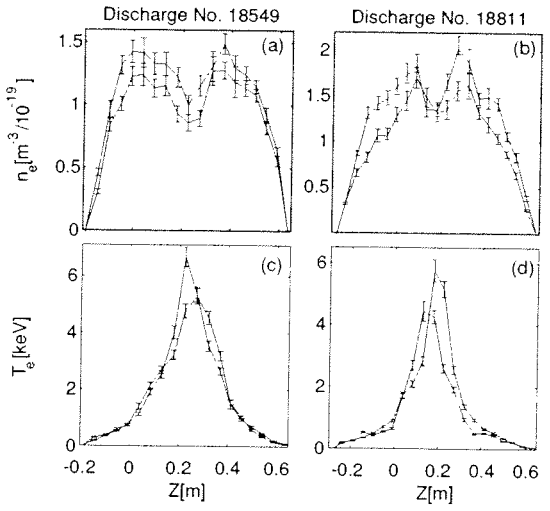

FIG. 5: Examples of electron density (a,b) and temperature (c,d) profiles (from Thomson scattering measurements) in a Co-ECCD (left) and a Counter-ECCD discharge (right). The profiles are shown at different times during mode activity revealing a kink displacement of the plasma core.

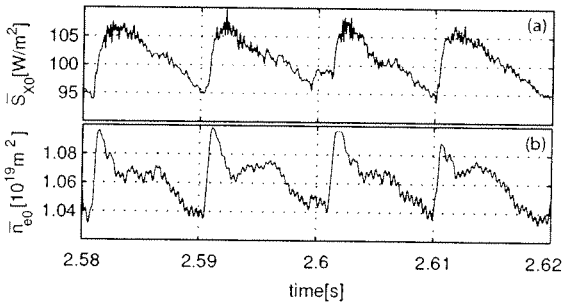

FIG. 6: Sawtooth behavior in TCV discharge No. 18549 where full current replacement with electron cyclotron Co-Cur rent drive was obtained with 2.7 MW of injected power. (a) Central line integrated soft x-ray emissivity. (b) Line integrated central density from a microwave interferometer operating at 140 GHz.

Both the Co- and the Counter-ECCD cases have steep electron temperature gradients in the core, Fig. 5(c,d), which are indicative of internal transport barriers (ITB's). ITB's in the electron transport channel have been observed in many ECH, Co- and Counter-ECCD scenarios in TCV and when they have been optimized to be MHD quiescent, do not have hollow density profiles[13–16] as shown in Fig. 8. In this figure, two examples are presented in which the $m = 1$ mode activity is suppressed by optimizing the deposition of the ECH power and the EC-driven current profiles. No $m = 1$ activity is observed on the soft x-ray signals, nor a rotating core displacement is apparent on temperature and

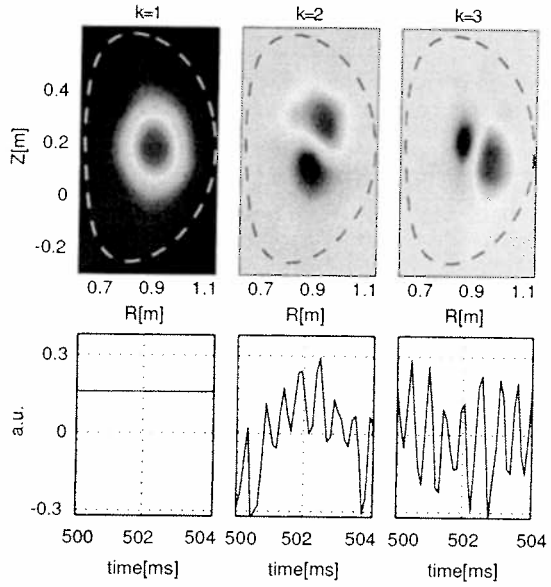

FIG. 7: SVD analysis of the reconstructed soft x-ray emissivities in TCV Counter-ECCD discharge No. 18811. Shown are the topo/chrono pairs corresponding to three largest eigenvalues. The top row shows the spatial eigenmodes (topos) with the last close flux surface (dashed line). The corresponding temporal eigenvectors (chronos) are shown in the bottom row.

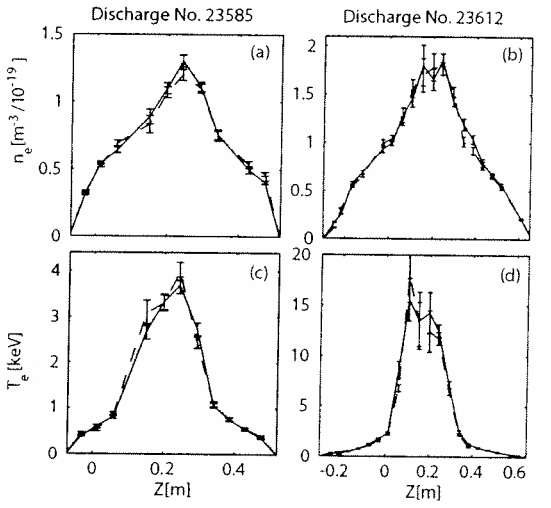

FIG. 8: Examples of electron density (a,b) and temperature (c,d) profiles (from Thomson scattering measurements) in a Co-ECCD (left) and a Counter-ECCD discharge (right). The deposition of the ECH power and the EC-driven current profiles were optimized to suppress $m = 1$ mode activity. Electron temperature profiles at different times during the discharges reveal no displacement of the core.

density profiles measured at different time during the discharge.

In Fig. 8(a,c), the plasma current $I_p = 105$ kA is fully EC driven for 4 seconds using two gyrotrons simultaneously, each delivering 0.45 MW of radio frequency power to the plasma. One gyrotron is aimed on-axis, whilst the other is aimed at $\rho \approx 0.3$ in order to achieve a sawtooth-free and MHD-quiescent discharge. Any possibility of Ohmic induction is suppressed by clamping the current in the Ohmic transformer as described in Ref. [17]. The superimposed profiles shown in Fig. 8(a,c) are obtained 3.9 and 3.95 s after the loop voltage is forced to be zero. The ECCD phase of this discharge is maintained for at least 10 current redistribution times. An estimate of the current redistribution time is obtained from the evolution of the plasma parameters from the initial ohmic condition to the fully EC driven plasma. The plasma current and the normalized internal inductance increase respectively from 90 kA to 105 kA and from 1 to 2 within 0.4 s after substitution of the ohmic current by ECCD. After this phase, plasma parameters are constant for the remaining 3.6 s of the ECCD pulse, ensuring that any residual of the ohmic electrical field has decayed away. Density profiles remain stationary and peaked throughout the discharge, i.e. for 10 current redistribution times at zero loop voltage, excluding any possibility of a contribution of the Ware pinch to the observed density peaking. Therefore, the origin of this convection must be an anomalous inward pinch for $\rho > 0.4$, where typical low confinement mode (L-mode) conditions are observed, and possibly a combination of anomalous and neoclassical inward pinches closer to the plasma center.

In Fig. 8(b,d), electron temperature and density profiles are shown in a sawtooth-free, MHD-quiescent plasmas with an electron ITB obtained with on-axis Counter-ECCD, using 3 gyrotron (1.4 MW), together with off-axis ECH using two gyrotrons depositing their power at $\rho \approx 0.3$. Unlike the case in Fig. 5(b,d), which only has central Counter-current drive, this discharge is free of $m = 1$ modes and has a peaked density profile. The slight steepening of the density profile in the core region, where electron temperature profile are steepest, in both cases in Fig. 8, is suggestive of inward thermodiffusion.

IV. DISCUSSION

The particle fluxes can generically be described by the transport equation $\Gamma = -D\nabla n + Vn + S$, where D is the particle diffusion coefficient, V a convective velocity and S a source term. In a source-free plasma, the density profiles evolve towards steady state profiles, determined by the balance of diffusive and convective fluxes satisfying the relation $\nabla n/n = V/D$.

Density profiles in tokamaks are ordinarily moderately peaked, corresponding to a negative (inward directed) convective velocity. In toroidal axisymetric geometry, inward particle convection can result from several phys-

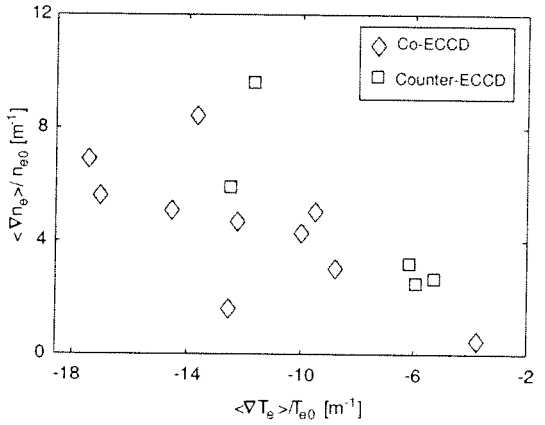

FIG. 9: Average n_e versus average T_e gradients over the region with hollow n_e profiles for Co- and Counter-ECCH cases.

ical mechanisms, such as neoclassical thermodiffusion [18], the Ware or the Varma pinches[19, 20], anomalous thermodiffusion[21–23] and the curvature driven pinch[23–25] (often referred to as curvature pinch) for which $V \approx -D\nabla q/q$. These mechanisms give rise to inward convection respectively when $\nabla T < 0$, $E_{tor}/B_{pol} > 0$ and $\nabla q > 0$. These conditions are fulfilled in virtually all positive shear tokamak discharges. There is evidence[26] that anomalous pinches, which are driven by turbulent fluctuations, are dominant in the 'confinement zone' (outside the inversion radius in sawtoothing discharges), but in principle, all four effects should be considered in the plasma core, where anomalous transport is generally reduced. Among these, only the curvature pinch offers the possibility of a density gradient reversal provided that the magnetic shear is reversed too. It can however be ruled out, since the ECH experiments presented in Figs. 1-4, as well as the fully ECCD discharge in Figs. 5,8(a,c), have positive shear, while discharges with central counter-ECCD or off-axis co-ECCD[16] have a reversed shear in the core.

Flattening of the density profiles in the presence of localized core heating, albeit without gradient reversal, was first reported, for the L-mode, in the ISX-B[27] and JFT-2[28] tokamaks and recently, for the High confinement mode, in the ASDEX-Upgrade[29] tokamak. In all cases, the phenomenon was attributed to an increased particle diffusivity. According to Ref. [30], the ECH can cause toroidal trapping of electrons by increasing the perpendicular energy of electrons of low parallel velocity. This leads to an excess of banana-electrons and thereby a poloidal charge asymmetry which produces a net electric field oriented in the direction of the major radius ("banana pile-up"). The resulting increased ion vertical drift velocity, by widening ion orbits, would then increase the neoclassical diffusivity. The explanation for ASDEX-Upgrade[29] was based on a conjecture of a link between anomalous particle and heat diffusivities with $D_e \approx 0.1\chi$. The increased local heat deposition by ion cyclotron resonance heating or ECH leads to a drastic increase of diffusivity, which, if the inward convection is assumed to be due to the Ware (or Varma) pinch, can explain the flattening of the density profiles. Although the above processes may well play a role, they are clearly not sufficient to explain the observation of hollow profiles. Hollow density profiles have not been reported from tokamaks other than TCV, possibly because the lower ECH power densities available on other devices may be below the threshold suggested by Fig. 4 or because of the absence of continuous kink modes.

Hollow density profiles are frequently observed in stellarators and attributed to neoclassical thermodiffusion of locally trapped particles [31]. Locally trapped particles are the hallmark of non-axisymetrical confinement and do not exist in an ideal (ripple and mode-free) tokamak. Unlike axisymetrical systems, neoclassical thermodiffusion in the presence of locally trapped particles is associated with a positive convective velocity, i.e, particles are expelled from regions with a strong temperature gradient[18]. The observations presented in this article may be understood as resulting from a balance of outward convection due to non-axisymetrical thermodiffusion and inward convection resulting from axisymetrical pinches, the former being dominant in the helically displaced, stellarator-like core. The same role could of course be played by an anomalous counterpart to non-axisymetrical neoclassical thermodiffusion, if such an effect exists and has the required sign. An explanation based on thermodiffusion is supported by the observation, made over several discharges with hollow density profiles, that there is a correlation between the density gradients and the temperature gradients, as shown in Fig. 9. Another possibility may be that absorbtion of perpendicular energy causes electrons to be trapped in the local mirrors and lost from the discharge core. In this case it remains to be explained why the phenomenon should be observed with ECCD, when the waves interact with electrons have a substantial parallel velocity. So far outward convection has only been observed in the presence of an $m = 1$ mode. Although there are only few examples of higher order modes affecting the plasma core, it is plausible that outward convection from the core may not occur with higher order modes, since, for symmetry reasons, they produce little or no helical displacement of the magnetic axis and hence no locally trapped particles.

V. CONCLUSIONS

In the TCV tokamak, inward or outward convection in the core of ECH and ECCD plasmas is observed, depending on discharge conditions. In sawtoothing discharges with central ECH, the outward convection is accompanied by a $m/n = 1/1$ rotating mode and results in inverted sawteeth of the central electron density. Suppression of this mode can be achieved by increasing the tri-

angularity and also by optimizing the deposition of the ECH power and the EC-driven current profiles. When sawteeth are stabilized, in the presence of a continuous $m = 1$ mode or a magnetic island, the outward convection results in stationary hollow electron density profiles and its occurrence is independent of the parallel velocity of the electrons interacting with the microwave beam. The occurrence of hollow density profiles in the presence of both helical displacements of the plasma core and steep electron temperature profiles supports an interpretation based on thermodiffusion in the presence of locally trapped particles.

Conversely, when the plasma is MHD-quiescent and hence axisymetrical, steep electron temperature profiles are associated with peaked density profiles and hence inward particle convection. The irrelevance of the sign of the local shear in the core suggests that this convection too, is thermodiffusive rather than due to the curvature pinch. The signs of the convective fluxes in both the axisymetrical and the helical core plasmas are in qualitative agreement with neoclassical predictions for thermodiffusion dominated by the presence of toroidally, respectivelly locally, trapped particles. The observations do not rule out the possibility that anomalous pinches may play a role. However, a simple increase of particle diffusivity due to ECH in the presence of a fairly constant Ware pinch cannot account for particle losses from the core, as observed in the presence of an $m = 1$ mode, since it cannot lead to the formation of hollow density profiles. We can also safely exclude the possibility that the Ware pinch plays a role in the inward pinch observed in quiescent fully ECCD plasmas, which have zero loop voltage. Since the heat transport in these discharges is anomalous over most of the cross section, an anomalous inward pinch is required to explain density profile peaking, at least in the outer half of the discharge. Density peaking in the core of quiescent fully ECCD plasmas, where transport is lower than in the periphery, may be due to neoclassical thermodiffusion, to an anomalous pinch, or a combination of thereof.

VI. ACKNOWLEDGEMENTS

The authors are grateful for support from the *Fond National Suisse pour la Recherche Scientifique*. I. Furno is now supported by the *Los Alamos Laboratory Directed Research and Development - Exploratory Research* program.

[1] F. Hofmann, J.B. Lister, M. Anton *et al.*, Plasma Phys. Controlled Fusion **36**, B277 (1994).
[2] T. P. Goodman, in *Proceedings of the 19th Symp. on Fusion Technology, Lisbon, (North-Holland, Amsterdam 1997)* (1996), vol. 1, p. 565.
[3] G. Smith, in *Electron Cyclotron Resonance Heating, 9th Joint Workshop* (1996), vol. 1, p. 651.
[4] M. Anton, M. J. Dutch, H. Weisen, Rev. Sci. Instrum. **66**, 3762 (1995).
[5] M. Anton, H. Weisen, M. J. Dutch *et al.*, Plasma Phys. Controlled Fusion **38**, 1849 (1996).
[6] T. D. de Wit, A. L. Pecquet, J. C. Vallet, R. Lima, Phys. Plasmas **5**, 3288 (1994).
[7] I. Furno, C. Angioni, F. Porcelli *et al.*, Nucl. Fusion **41**, 403 (2001).
[8] I. Furno, Ph.D. thesis, Ecole Polytechnique Fédérale de Lausanne (2001).
[9] R. Behn, in *Proceedings of the 7th Int. Symp. Laser Aided Plasma Diagnostics, Montreux, 2002* (1995), vol. 26B, p. 392.
[10] H. Weisen, J. M. Moret, S. Franke *et al.*, Nucl. Fusion **37**, 1741 (1997).
[11] H. Reimerdes, A. Pochelon, O. Sauter, T. P. Goodman, M. A. Henderson, A. Martynov, Plasma Phys. Controlled Fusion **42**, 629 (2000).
[12] O. Sauter, M. A. Henderson, F. Hofmann *et al.*, Phys. Rev. Letters **84**, 3322 (2000).
[13] Z. A. Pietrzyk, C. Angioni, R. Behn *et al.*, Phys. Plasmas **7**, 2909 (2000).
[14] Z. A. Pietrzyk, C. Angioni, R. Behn, S. Coda, T. P. Goodman, M. A. Henderson, F. Hofmann, O. Sauter, Phys. Rev. Letters **86**, 1259 (2001).
[15] T. P. Goodman, in *Proceedings of the 29th EPS Conference of Plasma Phys. and Contr. Fusion, Montreux, 2002* (2002), vol. 26B, p. 2.081.
[16] M. Henderson, to be published in Phys. Plasmas.
[17] S. Coda, T. P. Goodman, M. A. Henderson *et al.*, Plasma Phys. Controlled Fusion **42**, B311 (2000).
[18] L. M. Kovrizhnykh, Nucl. Fusion **24**, 851 (1984).
[19] A. A. Ware, Phys. Rev. Letters **25**, 916 (1970).
[20] R. K. Varma, Plasma Phys. Controlled Fusion **41**, 1053 (1998).
[21] F. Miskane and X. Garbet, Phys. Plasmas **7**, 4197 (2000).
[22] F. Jenko, Phys. Plasmas **7**, 514 (2000).
[23] J. Weiland, *Collective modes in inhomogeneous plasmas* (IOP Publishing Ltd 2000, 2000).
[24] D. Baker and M. Rosenbluth, Phys. Plasmas **5**, 2936 (1998).
[25] X. Garbet, to be submitted to Phys. Rev. Letters.
[26] A. Zabolotsky, to be published in Plasma Phys. Controlled Fusion.
[27] R. M. Gilgenbach, M. E. Read, K. E. Hackett *et al.*, Phys. Rev. Letters **44**, 647 (1980).
[28] R. J. LaHaye, T. Yamagishi, M. S. Chu, M. S. Schaffer, W. D. Bard, Nucl. Fusion **21**, 1425 (1981).
[29] J. Stober, O. Gruber, M. Kaufmann, R. Neu, F. Ryter, W. Sandmann, H. Zohm and the ASDEX Upgrade team, Plasma Phys. Controlled Fusion **44**, A159 (2002).
[30] J. Y. Hsu, V. S. Chan, R. W. Harvey, R. Prater, S. K. Wong, Phys. Rev. Letters **53**, 564 (1984).
[31] H. Ringler, U. Gasparino, H. Maassberg *et al.*, Plasma Phys. Controlled Fusion **32**, 933 (1990).

Observation and empirical modelling of the anomalous particle pinch in TCV

A. Zabolotsky, H. Weisen and TCV Team
Centre de Recherches en Physique des Plasmas,
Association EURATOM - Confédération Suisse,
Ecole Polytechnique Fédérale de Lausanne
CH-1015 Lausanne, Switzerland

ABSTRACT. Moderately peaked electron density profiles are observed in virtually all plasma conditions in TCV. The existence of an anomalous pinch is unambiguously demonstrated by the observation of peaked density profiles in stationary, fully relaxed, fully current driven ECCD discharges with V_{loop}=0. The behaviour of the density profiles from a database of 300 Ohmic L and H-mode, as well as ECH and ECCD discharges, is compared to predictions of models based on the Ware pinch, the curvature pinch and anomalous Thermodiffusion. Best overall agreement throughout the database is obtained with models combining an anomalous pinch mechanism, such as the curvature pinch, with the Ware pinch.

Introduction

It is generally assumed that peaked electron density profiles in tokamak plasmas, which are dominated by turbulent transport, exist due to an inward particle pinch [1]. However, the nature of this pinch remains unknown. A variety of the mechanisms responsible for anomalous pinch have so far been proposed. Neoclassical theory predicts a pinch proportional to the loop voltage, the so called Ware pinch [2]. Turbulent transport models [3-8] predict a pinch proportional to the temperature gradient (Thermodiffusion) and a pinch proportional to the gradient of the safety factor (Turbulent Equipartition or curvature pinch).

The TCV tokamak (R_0=0.88 m, a<0.25 m, B_T<1.5 T, I_p<1.1 MA) is well suited for density profile studies due to its wide range of equilibria, which allows the exploration of many different plasma conditions [9]. TCV is equipped with a very flexible and powerful electron cyclotron heating (ECH) and electron cyclotron current drive (ECCD) system [10].

Electron density profiles in sawtoothing TCV discharges are observed to be peaked. It is also noted in a wide variety of steady-state TCV tokamak discharges that the electron density profile peaking depends on the current profile peaking via the current profile width parameter $<j>/j_0 q_0$, irrespective of the electron density or plasma shape. In ECH plasmas, an additional dependence of the profile width on ECH power is found. To explain this density profile behaviour, the three above mentioned pinch mechanisms, Thermodiffusion, Turbulent Equipartition and the Ware pinch have been tested. For this purpose, the particle balance equation with an anomalous diffusion D and an apparent inward convective pinch V

$$\Gamma = -D\nabla n_e + Vn_e$$

where the Γ represents the particle flux and V contains all non-diagonal terms of the transport matrix, was expanded under steady-state conditions according to the formalism of each model:

$$\frac{1}{n_e}\frac{\partial n_e}{\partial \rho} = \frac{1}{<|\nabla \rho|> D(\rho)}\frac{V_{ware}}{} + \eta q H \frac{\partial}{\partial \rho}\frac{1}{qH} + \alpha \frac{1}{T_e}\frac{\partial T_e}{\partial \rho} + \hat{\Gamma}_s(\rho)$$

In this equation α and η are Equipartition and Thermodiffusion coefficients respectively, V_{ware} is the anomalous Ware pinch velocity, q is the safety factor, $\hat{\Gamma}_s$ represents the term related to particle source and $< >$ means an average over the flux surface. The geometrical factor $H=B_0 dVol/(2\pi R_0 d\Phi)$, where Vol, Φ, B_0 and R_0 are the plasma volume, toroidal flux, toroidal magnetic field and major radius at the magnetic axis respectively, is equal to unity in the large aspect ratio limit [5]. We assumed all plasma parameters to be constant on the flux surfaces, labelled by ρ. The main goal of the study is to abstract from the origin of turbulences responsible for the anomalous pinch in order to find the empirical transport coefficients, of the above form, which best fit the observations. As a result, the rest of the paper is organized as follows. Section 2 is dedicated to a presentation of the experimental density profiles and the observed behaviour in different discharge conditions. In Sections 2, 3 and 4 the results of the tests of each of the three above-mentioned mechanisms against the experimental data are presented and discussed. In Section 5 an interpretation based on a mixture of different mechanisms is proposed. Section 6 is dedicated to the summary and discussions.

1. Experimental Observations

The database of electron density profiles presented here consists of stationary, sawtoothing, positive shear Ohmic L-, Ohmic H- and ECH L-mode plasmas in TCV. All density and electron temperature profiles were measured using a repetitively pulsed Thomson Scattering system providing measurements along a vertical chord [11]. The measurements were mapped and fitted as smooth functions of the flux surfaces given by the LIUQE equilibrium code [12]. Figure 1A shows representative normalised experimental density and temperature profiles in Ohmic L-mode plasmas with two examples of observed density peaking as a function of $\rho = \sqrt{Vol/Vol_{tot}}$, where Vol is the volume enclosed by the flux surface. These examples show that the density profiles in TCV are indeed peaked.

In order to understand the profile behaviour in a variety of discharge condition, we found it useful to analyse the profiles in terms of their profile peaking widths. Sawteeth instabilities result in a flattening of the profile inside the sawtooth inversion radius and lead to a scatter of the core Thomson measurements taken at random times in the sawtooth cycle. In order to reduce such uncertainties in the analysed profiles we used "clipped" density profile widths, defined as $<\bar{n}_e>/n_{e1}$ where n_{e1} is the electron density at the sawtooth inversion radius, $n_e=n_{e1}$ for $r<r_{inv}$ and $n_e=n_e$ for $r \geq r_{inv}$ [13]. The values of inversion radius were obtained from a 200 channel soft X-ray system. Using these "clipped" profile peaking factors we were are only concerned with the profiles in the confinement zone, where they can be considered as being in steady state. We found that these peaking widths are best correlated with the current profile width defined by the parameter $<j>/j_0q_0$. Here $<j>$ is a cross-sectional average toroidal current density and $j_0q_0 = B_0 (k_0+1/k_0) /(\mu_0 R_0)$, where k_0, B_0 and R_0 are the elongation, toroidal magnetic field and major radius respectively at the magnetic axis. Since $<j>/j_0q_0 \cong 1/q_a$ in circular discharges (neglecting diamagnetic and paramagnetic corrections to the equilibrium field), this parameter can be considered as an effective cylindrical safety factor.

The scaling of "clipped" widths with $<j>/j_0q_0$ is shown in Fig. 1B for a wide variety of sawtoothing Ohmic L-mode discharges in TCV: $2 \cdot 10^{19}$ m^{-3} < n_{e1} < $14 \cdot 10^{19}$ m^{-3}, 2.5 < q_{95} < 7, 0.1 < ν^*_{75} < 10, 1 < κ_a < 2.6, -0.5 < δ_a < 0.7, where κ_a and δ_a are the elongation and the triangularity at the last closed flux surface and ν^*_{75} is the electron collisionality at 75% of the poloidal flux. Density profiles are shown to become flatter while $<j>/j_0q_0$ increases, indicating a correlation

between the density widths and the current profile. Different symbols on the figure refer to the classes of central electron density, demonstrating the fact that the profile widths and hence the profiles themselves are practically independent of the absolute value of the density, which determines the penetration of neutrals. This behaviour shows that the particle source term can be ignored in the particle balance equation in analysis of experimental scaling. The widths were also observed to be independent of plasma shape [13].

Although Ohmic H-modes are regularly obtained in a wide variety of TCV plasmas ($6{\cdot}10^{19}$ m^{-3} < n_{el} < $12{\cdot}10^{19}$ m^{-3}, 1.4 < κ_a < 2, 3.5 < q_{95} < 5, 0.3 < δ_a < 0.7), the range of $<j>/j_0q_0$ is smaller than for Ohmic L-modes. Figure1C shows the density peaking of Ohmic H-mode discharges together with the L-mode discharges. Over the available range of $<j>/j_0q_0$ the density peaking of H-mode discharges is very similar to L-mode discharges with the same $<j>/j_0q_0$. A direct comparison of the density profiles in L- and H- mode is possible since in TCV Ohmic H-mode there is no contribution of NBI to the particle source term. The fact that H-mode and L-mode discharges are similar in density peaking is surprising since the profiles of the diffusion coefficient in H-mode is generally assumed to be different from that in L-mode [14,15].

Experiments with additional heating were conducted using up to 6 gyrotrons operating at a frequency of 82.7 GHz corresponding to the second electron cyclotron frequency harmonic in TCV. The ECH data spans a range of $0.9{\cdot}10^{19}$ m^{-3} < n_{el} < $3{\cdot}10^{19}$ m^{-3}, 0.02 < ν^*_{75} < 1, 1.2 < κ_a < 2.3, 3 < q_{95} < 20. All discharges were limited sawtoothing L-modes with power up to 2.7 MW (up to thirteen times the power of the Ohmic target discharges). Due to the flexibility of the TCV ECH launching system, the data includes cases with pure ECH and cases with substantial electron cyclotron current drive, both in co and counter directions. The power absorption position varies from on- axis to off-axis heating. The dependence of the density peaking factor on the parameter $<j>/j_0q_0$ is shown in Fig. 1D. The symbols refer to classes of the ratio of the ECH power to the power in the Ohmic target discharge. At high ECH power, the profile widths behaviour becomes more complex and the inverse effective safety factor is no longer the dominant scaling parameter. A closer look at the data reveals an additional dependence on the ratio P_{ECH} / P^*_{OH}, where P^*_{OH} is the power in the corresponding Ohmic target discharge. In the presence of ECH, the scaling with the parameter $<j>/j_0q_0$ is similar to the Ohmic case only at $<j>/j_0q_0$ > 0.35 where the ratio P_{ECRH} / P^*_{OH} is less than 4. In this region the ECH density profiles are slightly broader, as shown in Fig. 1D in comparison with the average profile widths in corresponding Ohmic discharges.

Increasing the additional power leads to a flattening of the density profile, resulting in a deviation from the Ohmic scaling. The scatter of the data at high power can be partly explained by larger uncertainties of the Thomson scattering measurement at the low densities, which are typical for high power ECH in TCV. However, we cannot exclude the influence of other effects related to the different discharge regimes presented. It is for instance in the region $\langle j \rangle / q_0 j_0 < 0.35$ that the difference in collisionality between the ECH dataset and the Ohmic dataset is largest. Despite this scatter, the profiles become in general broader as the ECH power increases.

2. Testing the Ware Pinch

The Ware pinch effect arises from the interaction of the parallel electric field with the trapped particles in banana orbits [2]. The corresponding drift velocity is $V_{ware} = E_{//} / B_\theta$, where $E_{//}$ is the toroidal electric field and B_θ is the poloidal magnetic field. In order to derive $\nabla n / n$ from the particle balance equation one has to choose the value of D, which a priori is unknown. However, it was observed that there might be a relation between heat and particle diffusivities [16,17]. Therefore, the particle diffusion coefficient is usually chosen to be proportional to the heat diffusion coefficient. For example ASDEX reports [18] that, at least in some cases, it is sufficient to invoke the Ware pinch together with a diffusion coefficient which is typically 1/4 of the electron heat diffusivity to explain the observed density peaking.

The Ware pinch involves only the trapped particles, thus to obtain the effect on the plasma as a whole this velocity has to be corrected for the trapped particle fraction in a collisional plasma $V_{ware} = f_t f_v E_{//} / B_\theta$. The profile of the velocity, the fraction of the trapped particles f_t and a factor f_v takes into account the effect of collisions, were calculated using the experimental data in the approximation of a nested circle geometry. Profiles of the effective heat diffusion coefficient χ were obtained from the power balance $\chi = Q_{tot} / n_e \nabla T_e < |\nabla \rho| >$ and assuming a direct connection between heat and particle transport, D was chosen proportional to χ.

Figure 2A shows the experimental density profiles for Ohmic L-mode discharges together with the profiles expected from the Ware pinch with different assumed ratios D/χ. For these examples, the Ware pinch alone provides sufficient peaking if the ratio D/χ is about 0.2-0.3. Although the details of the profile are not well matched, discrepancies may be explained by uncertainties in the numerous parameters used for the Ware pinch calculations or inaccuracy due to simplifications

used. In Fig. 2B the experimental scaling of the density widths is compared with the scaling predicted by the Ware pinch. The lines correspond to a fit of the widths calculated with the Ware pinch for each discharge. The experimental behaviour of the profile widths is described by the Ware pinch model if the ratio D/χ lies in the range from 0.2 to 0.3. Such values of D/χ are in agreement with the results obtained on ASDEX in Ohmic H-mode shots [18,19].

Figure 2C shows the experimental profile in a discharge with 450 kW of ECH power. In the case of pure ECH heating, the profile given by the Ware pinch with the same value of D/χ as for the Ohmic cases strongly deviates from the experimental one. In order to match the experimental profile in Fig. 2C the D/χ ratio should be about 0.05, which is four times lower than the average in Ohmic discharges. In the discharge presented, χ at the edge is about 5 m^2/s. Taking into account the coefficient of proportionality between D and χ obtained, the particle diffusion coefficient at the edge should be about 0.25 m^2/s. This value is significantly lower than the value of D observed in other tokamaks [14,15].

An unambiguous test of the applicability of the Ware pinch in TCV discharges was obtained by investigating discharges with fully sustained current drive. In these discharges, there is no Ohmically driven current and hence there is no parallel electrical field [20]. According to the Ware pinch model, the density profile should become completely flat. Figure 2D shows an example of a profile observed in a discharge with a fully non inductively driven current. This 107kA discharge was fully EC driven for 4 seconds using two gyrotrons at any time, each delivering 0.45MW of RF power to the plasma. The gyrotrons were aimed at the axis and at $\rho \approx 0.3$ in order to achieve a sawtooth-free and MHD-quiescent discharge. Any possibility of Ohmic induction was suppressed by clamping the current in the Ohmic transformer as described in ref [20]. The current redistribution time, inferred from the evolution of the internal inductance l_i at ECCD switch-on was 0.4 s, at which point l_i had settled to a constant value and hence the initial Ohmic toroidal electrical field had decayed away. Density profiles remained stationary and peaked throughout the discharge i.e. for 10 current redistribution times with $V_{loop}=0$, excluding any possibility of a contribution of the Ware pinch to the observed density peaking. Although the parallel electric field is absent the density peaking in this discharge does not change appreciably compared with the case of pure ECH heating where the electric field is about 0.25 V/m. Over all available data, in which the parallel electric field spans a range from practically 0 up to 0.25 V/m no influence of the electric field on the density peaking was observed.

In spite of the agreement between experiment and predictions in Ohmic discharges the Ware pinch mechanism cannot therefore be a dominant effect in TCV plasmas. Nevertheless, some flattening, with respect to the Ohmic discharges, is observed indicating that the Ware pinch may contribute to the peaking in Ohmic plasmas.

3. Testing the Turbulent Equipartition

Turbulent Equipartition (TEP) assumes the conservation of the second adiabatic invariant $J = \oint \sqrt{E - \mu B} dl$ (where E is the particle kinetic energy, B is the magnetic field and μ is the usual first adiabatic invariant) during turbulent transport [4]. As a result of this assumption, particles distribute themselves evenly over the poloidal flux, i.e. $\partial N/\partial \Psi \approx const$, where N is the total number of particles within a given flux surface. This distribution of the trapped particles over the flux surfaces when trapped and passing particles diffuse in the same way leads to a density roughly proportional to $1/qH$, where q is a safety factor. The difference in the diffusion of trapped and passing particles modifies the density profiles to $(1/qH)^{\eta}$, where $0.3 \leq \eta \leq 1$ depends on the relative contributions of trapped and passing particles to the particle transport [15]. The counterpart of TEP in fluid theory is the curvature pinch [8].

It was shown previously in Ohmic L-mode and ECH discharges, that in TCV N increases roughly linearly with Ψ, irrespective of other discharge parameters (see figures 10 and 11 in ref. [13]). The same effect is observed in the present extended data set both in Ohmic H-mode discharges and also in all ECH discharges independently of the additional power, injection angle or power deposition position.

Figure 3A shows examples of experimental Ohmic density profiles, together with the profiles obtained from TEP predictions using the q profiles given by the equilibrium reconstruction code. In the majority of the analysed Ohmic discharges the whole density profile in the confinement zone can be fitted by TEP with a single value of η close to 1. The scaling of the density peaking with the parameter $\langle j \rangle / q_0 j_0$ predicted by TEP with different values of η is shown in Fig. 3B by lines. Agreement with the experiments is reached in TCV Ohmic discharges if $\eta \sim 1$ suggesting that if TEP is a dominant pinch mechanism, trapped and passing particles should give a similar contribution to the particle transport in all Ohmic TCV discharges. This value of η is somewhat

higher than that obtained in Ohmic discharges in DIII-D where TEP alone can explain the observed peaking if η~0.7 [5,15].

Figure 3C and Fig. 3D illustrate that TEP also provides sufficient peaking in the case of ECH heating. For the broader density profiles in TCV ECH discharges, a good fit of the scaling in the range of effective inverse safety factor 0.4< $<j>/j_0q_0$ <0.6 (where the ECH power is limited to 3 times the Ohmic power) can be obtained if η is about 0.8 as shown in Fig. 3D. However, in the region $<j>/j_0q_0$ <0.3 where data are available at higher additional power TEP, with the same value of η, predicts profiles which are more peaked than the observed ones. It can be suggested that for any limited range of power it is possible to find a single η, which provides the correct scaling of the profile widths with $<j>/j_0q_0$. However, η must decrease while the profiles become broader. One possible explanation is that a change of the transport regime towards a more trapped particle dominated transport at high power should lead to a reduction of η within the framework of TEP.

Although the agreement between TEP and experiment is remarkably good in the Ohmic case, it is not satisfactory in the case of ECH heating if a single value of η is assumed.

4. Testing the Thermodiffusion

It has already been reported that in some TCV experiments the temperature profiles are correlated with the current profile [21]. In this case, turbulent thermodiffusion (TTD) can provide an alternative interpretation of the observed density profile scaling. The process of Thermodiffusion is based on a variation of the diffusion coefficient in phase space with the particle energy. It is expected to lead to steady state density gradients, which, in source free regions and in the absence of other pinch mechanisms, are proportional to the temperature gradients, such that $\nabla n/n = \alpha \nabla T/T$. The values of α depend on the strength of electrostatic turbulence assumed to be responsible for anomalous Thermodiffusion [3].

The profile details in L-mode Ohmic discharges and a TTD fit are compared in Fig 4A. The experimental Ohmic density profile widths and those calculated using TTD are presented in Fig. 4B. These examples show that TTD alone provides sufficient peaking for the majority of TCV Ohmic discharges if α is in the range 0.4-0.65, which is in a good agreement with the value α~0.5 found on ASDEX for Ohmically heated discharges [22]. However, the experimental widths decrease with $<j>/j_0q_0$ faster than the widths obtained from TTD with a unique value of α. This

means that α must itself be allowed to scale with $<j>/j_0q_0$ in order to reproduce the observations. Such a scaling suggests a relation with the q profile or shear.

In the case of ECH heating, we can roughly separate two classes. The first class corresponds to those discharges where the additional heating does not modify the radial behaviour of the temperature profile. In the second class, two main regions of the temperature profile with different gradients are observed. For the majority of the discharges of the first class, TTD provides a good fit of density profiles with single value of α close to 0.5 (Fig. 4C).

The experimental density and temperature profiles in the second class of discharges are presented on Fig 4D. For this example, the gradient of the temperature changes significantly at $\rho \approx 0.6$, however concomitant changes of the density profile are not observed. It is clear that with a single value of α TTD cannot fit the experimental density profile and changes of α at $\rho \sim 0.6$ are needed. For this particular discharge TTD provides a good description of the density profile if $\alpha \sim 0.2$ for $\rho < 0.6$ and $\alpha \sim 0.55$ for $\rho > 0.6$. Values of α close to 0.5 in the zone of low temperature gradient are found in practically all discharges with changes of the temperature gradient. For some cases α can be as low as 0.1 in the zone with a high temperature gradient. Such extreme cases can be attributed to discharges with an internal transport barrier (ITB). Discharges with pronounced ITB's where α can potentially be lower are not included in this paper because of the reversed shear typical of this kind of TCV discharges [23]. Changes of α as a function of radius may be related to the changes of the nature of the turbulence similar to those observed in discharges with an ITB [24].

To summarise, we conclude that TCV density profile peaking in the case of Ohmic discharges can be determined by Thermodiffusion alone if α itself scales with $<j>/j_0q_0$. In the ECH discharges, TTD provides sufficient peaking for the majority of the cases although changes of α along the radius are needed in order to explain the resilience of density profiles to changes in temperature scale length.

5. Testing the mixed interpretation

A natural next step of the present analysis is an attempt to use interpretations based on combinations of different mechanisms. As an example, Fig.5A and Fig.5B illustrate the results of such a combination, obtained by taking into account TEP with η=0.45 and a Ware pinch with

D/χ=0.4. Figure 5A shows that this model combination, provides a good match to the observed scaling of widths in the case of Ohmic L-mode. Additionally Fig. 5B illustrates that such an interpretation also reproduce the overall behaviour of the flattening with additional power.

While the above interpretation in general fits the observation, the correspondence between model predictions and experiment in TCV can also be obtained for mixture of Ware pinch and some linear combination of TTD and TEP partly because of the high degree of the correlation of $<T_e>/T_{e1}$ and $<j>/j_0q_0$ in the dataset [13]. As a result, based on the available data we cannot conclusively separate the influence of TTD and TEP on the density profiles.

6. Summary

Any single pinch model, which can be considered as a good candidate responsible for TCV electron density profile peaking should not only predict the profile details and peaking scaling with $<j>/j_0q_0$ in Ohmic cases but also explain the profile flattening with additional power. The conclusion we can make at this point is that none of the three mechanisms presented above can predict all of the observed features of TCV density profile behaviour with a single coefficient.

Despite the fact that the Ware pinch alone provides a good description of the density profiles in the case of Ohmic L- and H-mode discharges if the D/χ ratio is about 0.2-0.3, it fails to predict the profile peaking in TCV ECH discharges, in particular profiles in discharges with fully sustained current drive.

The density profiles in Ohmic discharges can be fitted by TEP alone if η is about 1. In the case of ECH heating, TEP matches the experimental profiles well, however a decrease of η is required to follow the flattening of the profiles as the fraction of additional power increases.

In Ohmic discharges TTD alone provides sufficient peaking for the majority of the discharges if $0.4<\alpha<0.6$ but additional scaling of α is needed to explain the observed scaling of density widths with the parameter $<j>/j_0q_0$. In ECH discharges, the modification of the temperature gradients by heating together with the stiffness of the density profiles lead to the necessity of changes of α with radius. TTD fits the density profiles in the ECH discharges with values of α from 0.1 to 0.5 depending on the temperature profiles.

Mixed interpretations can in general explain the profile behaviour in Ohmic and ECH discharges with a single set of coefficients but the present data do not allow us conclusively separate the contribution of each mechanism. Future work will be aimed at overcoming this difficulty by

performing experiments with modified profiles of the safety factor in the presence of additional ECH heating.

Acknowledgments

The authors gratefully acknowledge the support of entire TCV team. They would like also to thank X.Garbet, J.Weiland, J.B.Lister and D.R.Baker for helpful discussions and comments. This work was partly supported by the Swiss National Science Foundation.

References

[1] F.Wagner and U Stroth, Plasma Phys. Control. Fusion 35 (1993) 1321

[2] A.A.Ware, Phys Rev. Letters 25 (1970) 916

[3] F.Miskane and X.Garbet, Phys. Plasmas 7 (2000) 4197

[4] J.Nycander and V.V.Yancov, Phys. Plasmas 2 (1995) 2874

[5] D.R.Baker and M.N. Rosenbluth, Phys. Plasmas 5 (1998) 2936

[6] R.E. Waltz et al., Phys. Plasmas 4 (1997) 2482

[7] J. Weiland 'Collective modes in inhomogeneous plasmas' IOP Publishing Ltd, 2000, Bristol & Philadelphia, ISBN 0 7503 0589 4 hbk

[8] X. Garbet et al.,'Turbulent Particle Transport in Magnetized Plasmas' submitted to Phys. Rev. Lett. (2003)

[9] J.-M.Moret, et al., Proc. of the 29th EPS Conference on Plasma Physics and Controlled Fusion, Montreux (2002)

[10] T.P. Goodman et al., Proc. of the 19th Symposium on Fusion Technology, Lisbon (1996) 565

[11] R.Behn et al., Proc. of the 7th Int. Symp. Laser Aided Plasma Diagnostics, Fukuoka (2002) 392

[12] F.Hofmann et al., Nuclear Fusion 28 (1988) 1871

[13] H.Weisen et al., Nuclear Fusion 42 (2002) 136

[14] ITER Physics Basis Editors, Nucear Fusion 39 (1999) 2137

[15] D.R.Baker et al., Nuclear Fusion 40 (2000) 1003

[16] D.R.Baker et al., Nuclear Fusion 38 (1998) 485

[17] F.Ryter et al., Nuclear Fusion 41 (2001) 537

[18] J.Stober et al., Plasma Phys. Control. Fusion 44 (2002) A159

[19] J.Stober et al., Plasma Phys. Control. Fusion 43 (2001) 39

[20] S.Coda et al., Plasma Phys. Control. Fusion 42 (2000) B311

[21] H.Weisen and E.Minardi, Europhysics Letters 56 (2001) 542

[22] G.Becker, Nuclear Fusion 27 (1987) 11

[23] Z.A.Pietrzyk at al., Physical Review Letters 28 (2001) 1530

[24] E.J. Doyle et al., Nuclear Fusion 42 (2002) 333

[25] H.Weisen et al., Nuclear Fusion 41 (2001) 1227

[26] L.Garzotti et al., Proc. of the 29th EPS Conference on Plasma Physics and Controlled Fusion, Montreux (2002)

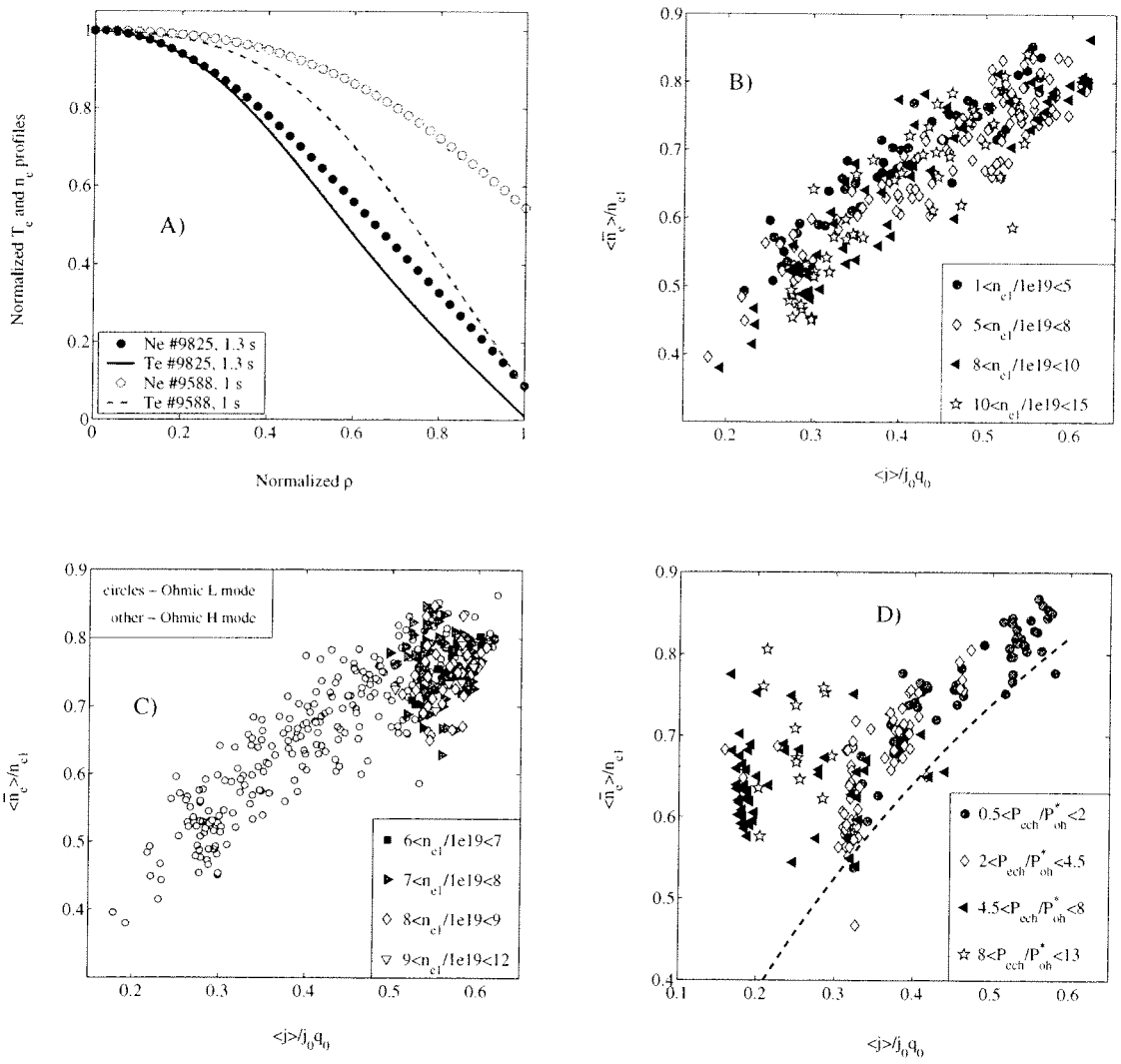

Fig. 1 **A)** Typical normalized electron density and electron temperature profiles observed in TCV Ohmic L-mode discharges. Discharge #9588 represents low TCV density peaking ($<j>/j_0q_0$=0.55, $<n_e>/n_{el}$=0.85, q_{95}=2.5) and discharge # 9825 high TCV density peaking ($<j>/j_0q_0$=0.23, $<n_e>/n_{el}$=0.44, q_{95}=5.9). **B)** Scaling of electron density inverse peaking factor for Ohmic L-mode discharges. The symbols refer to the class of the electron density at the inversion radius. **C)** Scaling of the electron density inverse peaking factor for both Ohmic L- and Ohmic H-mode discharges. The symbols refer to the class of the electron density at the inversion radius. **D)** Scaling of electron density inverse peaking factor for ECH discharges. Symbols refer to the class of ratio of ECH power to the Ohmic power of the target discharge. The dashed line shows the average inverse peaking factor for Ohmic discharges as a function of $<j>/j_0q_0$.

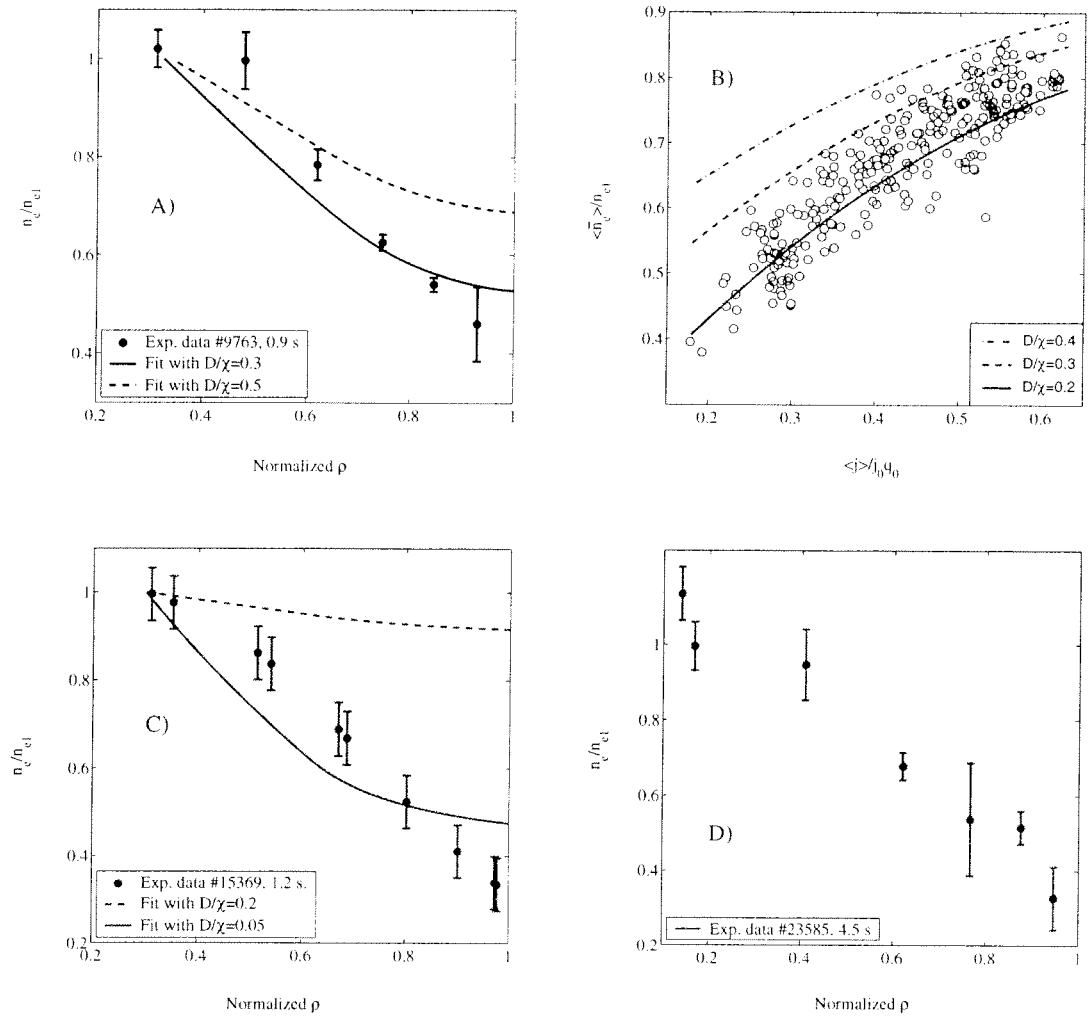

Fig. 2 **A)** Experimental density profile for Ohmic L-mode discharges (dots) together with profiles provided by the Ware pinch (lines) with different D/χ ratios assumed. Profiles are normalized to the density values at the inversion radius. **B)** Scaling of the electron density inverse peaking widths for Ohmic discharges (dots) and average widths predicted by the Ware pinch (lines). **C)** Density profile in an ECH discharge with 450 kW of heating power (dots) and the profile given by the Ware pinch model assuming different values of the D/χ ratio. Profiles are normalized to the density values at the inversion radius. **D)** Experimental density profile in an ECH discharge with fully sustained current drive. Heating power is 0.9 MW, current is 107 kA, $\langle j \rangle / j_0 q_0 = 0.17$, $\langle n_e \rangle / n_{e1} = 0.5$.

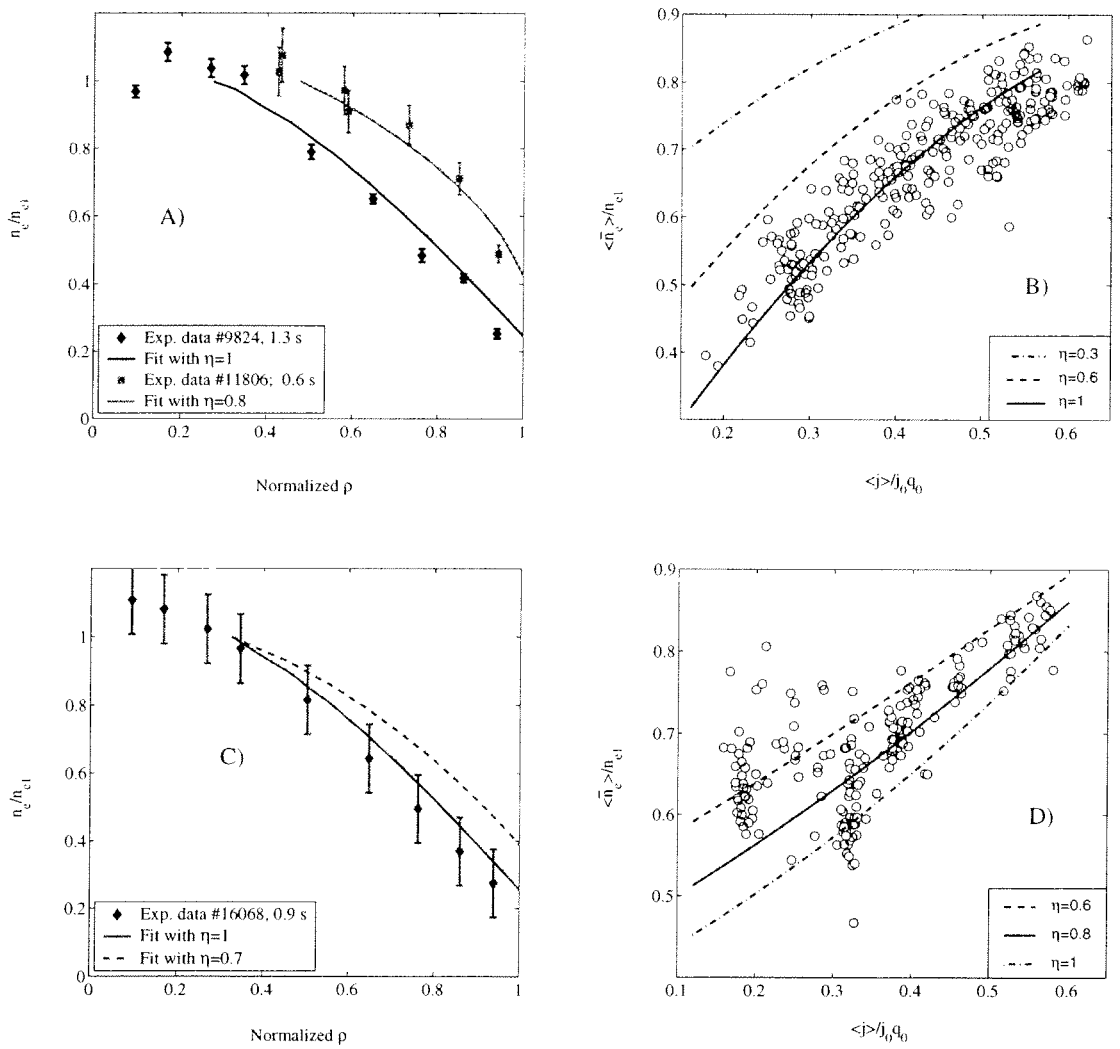

Fig. 3 **A)** Experimental density profile for Ohmic L-mode discharges (dots) and profiles predicted by TEP (lines). Profiles are normalized to the density values at the inversion radius. **B)** Scaling of electron density inverse peaking widths for Ohmic discharges (dots) and average widths predicted by TEP with different values of η (lines). **C)** Experimental density profile in ECH discharge (dots) and profiles predicted by TEP with two different values of η (lines). Profiles are normalized to the density values at the inversion radius. **D)** Experimental scaling of electron density inverse peaking factor in ECH discharges (symbols) and average widths predicted by TEP with three different values of η.

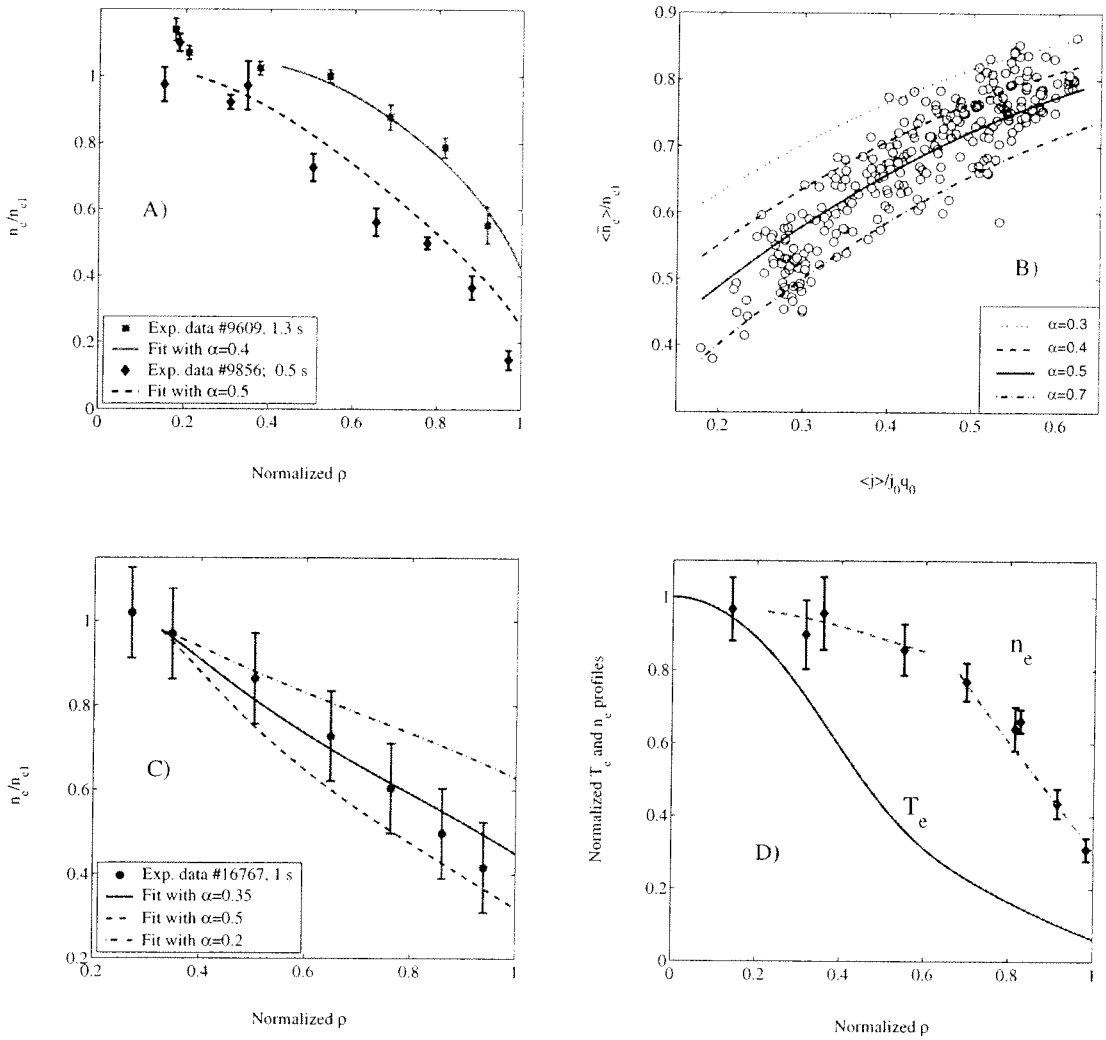

Fig. 4 **A)** Experimental density profiles in Ohmic L-mode discharges (dots) compared with a TTD predictions. Profiles are normalized to the density values at the inversion radius. **B)** Experimental scaling of electron density inverse peaking factor for Ohmic L-mode discharges (symbols) and scaling predicted by TTD with four different values of α. **C)** Experimental density profile in ECH discharge (dots) and profiles predicted by TTD with different values of α. Profiles are normalized to the density values at the inversion radius. **D)** Experimental normalized density and temperature profiles in counter ECCD discharge #15733 at time 1 s. ECH power is 0.9 MW, $\langle j \rangle / j_0 q_0 = 0.3$, $\langle n_e \rangle / n_{el} = 0.63$, inversion radius $\rho \sim 0.35$. Dashed line is TTD prediction with $\alpha = 0.2$, dash-dotted line is TTD with $\alpha = 0.5$. Profiles are normalized to the values at the plasma centre.

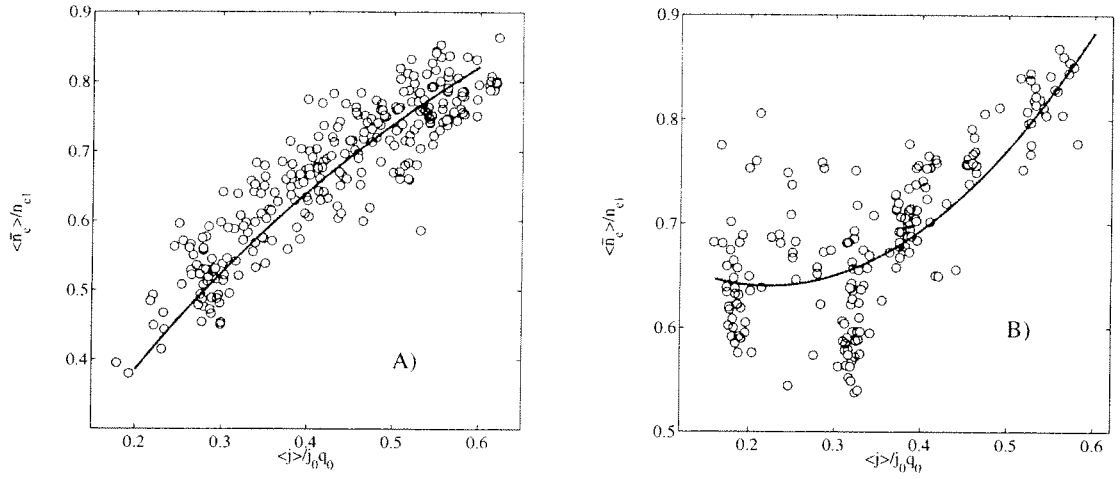

Fig. 5 **A)** Experimental scaling of inverse peaking factor for Ohmic L-mode discharges (symbols) and scaling predicted by combination of Ware pinch with D/χ=0.4 and TEP with η=0.45 (line). **B)** Experimental scaling of effective electron density inverse peaking factor for ECH discharges (symbols) and scaling predicted by combination of Ware pinch with D/χ=0.4 and TEP with η=0.45 (line).